Editors' Suggestion

Quantum Information Scrambling in a Trapped-Ion Quantum Simulator with Tunable Range Interactions

Manoj K. Joshi,[1,2] Andreas Elben,[1,2] Benoît Vermersch,[1,2,3] Tiff Brydges,[1,2] Christine Maier,[1,2] Peter Zoller,[1,2] Rainer Blatt,[1,2] and Christian F. Roos[1,2]

[1]*Center for Quantum Physics, University of Innsbruck, Innsbruck A-6020, Austria*

[2]*Institute for Quantum Optics and Quantum Information of the Austrian Academy of Sciences, Innsbruck A-6020, Austria*

[3]*University Grenoble Alpes, CNRS, LPMMC, 38000 Grenoble, France*

(Received 10 January 2020; accepted 29 May 2020; published 19 June 2020)

In ergodic many-body quantum systems, locally encoded quantum information becomes, in the course of time evolution, inaccessible to local measurements. This concept of "scrambling" is currently of intense research interest, entailing a deep understanding of many-body dynamics such as the processes of chaos and thermalization. Here, we present first experimental demonstrations of quantum information scrambling on a 10-qubit trapped-ion quantum simulator representing a tunable long-range interacting spin system, by estimating out-of-time ordered correlators (OTOCs) through randomized measurements. We also analyze the role of decoherence in our system by comparing our measurements to numerical simulations and by measuring Rényi entanglement entropies.

DOI: 10.1103/PhysRevLett.124.240505

Synthetic quantum systems of atoms, ions, and superconducting qubits provide us with excellent platforms for studying fundamental aspects of the quantum information dynamics [1]. Existing tabletop experiments with high fidelity quantum control have great prospects in exploiting features of quantum dynamics related to black holes and gravity models, high energy physics models and condensed matter systems [2–4]. These platforms can probe essential out-of-equilibrium phenomena of interacting many-body systems, such as quantum chaos, thermalization and many-body localization [5,6]. In particular, the systems with single-site control have demonstrated the spreading of time-ordered correlations [7–9] and they have confirmed the existence of Lieb-Robinson bounds [10] in nonrelativistic locally interacting systems [11,12].

Recently, a novel concept has been shown to have the ability to identify a fundamental feature of many-body quantum dynamics: quantum information scrambling. Here, "scrambling" describes how quantum information, initially encoded in terms of local operators, becomes, after time evolution, increasingly nonlocal and complex [13]. As a quantum version of the butterfly effect [14], scrambling can be identified with the decay of a new type of many-point correlation functions, namely, out-of-time ordered correlations (OTOCs) [15,16]. OTOCs have been first used to quantify the properties of "fast scrambling" governed by universal Lyapunov exponents in the dynamics of black holes [13,15–21], and to describe chaotic systems with holographic duals [22,23]. For quantum lattice models, which are more relevant to experiments with current quantum simulators, OTOCs have the form

$$O(t) = D^{-1}\mathrm{Tr}[W(t)VW(t)V], \tag{1}$$

with $W(t) = e^{iHt}We^{-iHt}$ a time-evolved Heisenberg operator, W and V local, Hermitian operators, H a many-body Hamiltonian and D the Hilbert space dimension [24]. OTOCs have been shown to detect universal signatures of many-body quantum chaos [25–27], many-body localization [28–30], and dynamical quantum phase transitions [31]. In particular, in ergodic systems with local interactions, the decay of the OTOCs of local operators W and V initially separated by a distance d occurs at a characteristic time $t_c \sim d/v_B$, where v_B is the butterfly velocity [19]. This result can be understood from a hydrodynamical description associated with a *ballistic* spatial spreading of the operator $W(t)$, whose "wave front" travels with velocity v_B and also broadens diffusively in time [25–27,32,33]. While in seminal experimental work, OTOCs have been measured either for *collective* (nonlocal) operators [34,35] or in small-scale 3–4 qubit systems [2,36], scrambling quantified by the OTOCs of local operators (encoding local quantum information) has so far eluded observation in a many-body system.

In this Letter, we present first measurements of OTOCs in a spin-model consisting of $N = 10$ qubits with local interactions of tunable range, realized in a trapped-ion quantum simulator. To this end, we implement a recently proposed protocol, based on measuring statistical correlations of randomized measurements [37], to access OTOCs as defined in Eq. (1). This allows us in particular to monitor the emergence of a traveling operator wave front, and observe the crucial role played by the interaction range

[38–43]. Furthermore, we demonstrate the robustness of the implemented protocol against certain types of decoherence mechanisms. Most importantly, the implemented protocol neither relies on time-reversed evolution nor auxiliary degrees of freedom required in previous proposals [44–49]. To verify its robustness, we compare our measurement results with numerical simulations, and perform additional randomized measurements of operator spreading [50], and entanglement Rényi entropies [51,52].

Experimental setup and protocol.—The experimental studies are performed on a trapped-ion analog quantum simulator, realized with a linear chain of $N = 10$ $^{40}Ca^{+}$ ions. Quantum information is encoded in two (pseudo-) spin states $|S_{1/2}, m = +1/2\rangle \equiv |0\rangle$ and $|D_{5/2}, m = +5/2\rangle \equiv |1\rangle$, respectively. Entangling operations are performed using a bichromatic laser field, which off-resonantly couples the electronic and vibrational states of the ions [8]. The resulting interaction Hamiltonian is expressed as

$$H = \sum_{i \neq j} \frac{J_0}{|i-j|^{\alpha}} \sigma_i^x \sigma_j^x + B \sum_i \sigma_i^z, \tag{2}$$

where i, j are the indices representing the position of ions in the chain, and $\sigma^{\beta}, \beta \in \{x, z\}$, denote Pauli spin matrices; J_0 and α represent the maximum strength and exponent of the equivalent Ising-type interaction, respectively. Note that the above interaction Hamiltonian leads to a spin *flip-flop* type interaction when the transverse field $B \gg J_0$ (i.e., $H = \sum_{i \neq j} J_{ij} \sigma_i^+ \sigma_j^- + B \sum_i \sigma_i^z$), which is routinely used in analog quantum simulators [8,9]. Coherent control of the spin state of an individual qubit is achieved by a tightly focused, steerable laser beam, enabling the preparation of any desired product state $|\Psi_k\rangle = \bigotimes_{i=1}^{N} |\psi_i\rangle$. More details about the experimental platform can be found in the Supplemental Material [53].

The experimental protocol to measure OTOCs consists of two main parts and is illustrated in Figs. 1(a) and 1(b). In the first part [Fig. 1(a)], we prepare an initial product state $|\mathbf{k}_0\rangle = |0, 0, \ldots, 0\rangle$. Next, we apply a local random unitary $u = u_1 \otimes \ldots \otimes u_N$ where each u_i, implementing a random single spin rotation, is sampled independently from the circular unitary ensemble [58]. As investigated in detail in Refs. [52,59], these unitaries are generated with high fidelity in our apparatus (see the Supplemental Material for single-qubit gate fidelity [53]). Subsequently, the system is evolved in the presence of the Ising Hamiltonian H, for time t and the operator $W = \sigma_j^x$, for $j \in \{1, \ldots, N\}$, is measured. After $N_M = 150$ ($N_M = 300$ for $t = 4$, 5 ms) repetitions, one obtains an estimation of $\langle W(t)\rangle_{u,\mathbf{k}_0} = \langle \mathbf{k}_0 | u^{\dagger} W(t) u | \mathbf{k}_0 \rangle$. In the second part of the experiment, we prepare the initial product state $|\mathbf{k}_0\rangle$ and repeat the experimental procedure with the same random unitary u. In this part, a unitary $V = \sigma_1^z$, is applied, in addition, before the time evolution [see Fig. 1(b)]. By repetition ($N_M = 150$ or $N_M = 300$), we obtain an estimation of $\langle VW(t)V\rangle_{u,\mathbf{k}_0}$. The steps are illustrated in Fig. 1(b). Both parts are finally repeated for $N_U = 500$ sets of unitaries u to build statistical correlations. Note that the choice of N_M and N_U determines the expected statistical error which is investigated in detail in Ref. [37].

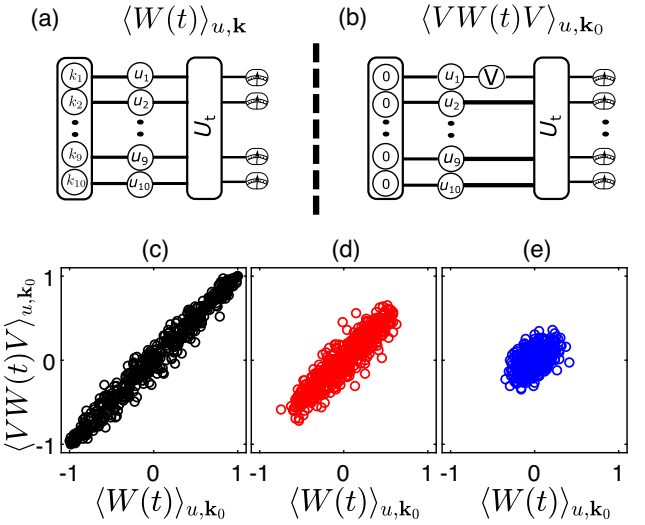

FIG. 1. (a),(b) Experimental procedure to measure two parts of the OTOCs $\langle W(t)\rangle_{u,\mathbf{k}}$ and $\langle VW(t)V\rangle_{u,\mathbf{k}_0}$. Here, $\mathbf{k}$ ($\mathbf{k}_0$) refers to the initial product state $|\mathbf{k}\rangle = |k_1, k_2, \ldots, k_n\rangle$ ($|\mathbf{k}_0\rangle = |0, \ldots, 0\rangle$) with $k_i \in \{0, 1\}$. (c)–(e) Spread of operator $W(t) = \sigma_5^z(t)$ is observed in terms of loss of correlations between two measured quantities ($\langle W(t)\rangle_{u,\mathbf{k}_0}$ and $\langle VW(t)V\rangle_{u,\mathbf{k}_0}$) for $t = 0$, 2, and 5 ms, where $V = \sigma_1^z$. The experimental study is carried out for $\alpha = 1.21$, $J_0 = 2\pi \times 30.13$ Hz and $B = 2\pi \times 1.5$ kHz (see the Supplemental Material for the experimental details [53]).

The basic intuition to understand how statistical correlations between two randomized measurements $\langle W(t)\rangle_{u,\mathbf{k}_0}$ and $\langle VW(t)V\rangle_{u,\mathbf{k}_0}$ can be used as probes for operator spreading, and how they are related to OTOCs is provided in Figs. 1(c)–1(e). The figure shows experimentally measured expectation values $\langle W(t)\rangle_{u,\mathbf{k}_0}$ and $\langle VW(t)V\rangle_{u,\mathbf{k}_0}$ for $N_U = 500$ unitaries u, $V = \sigma_1^z$ and $W = \sigma_5^x$. At initial time $t = 0$ ms [Fig. 1(c)], the system has not evolved under H, and so the measurement of W at $j = 5$ is not affected by whether V has been applied at $j = 1$ or not. Thus, we observe (up to projection noise) near perfect correlations between $\langle W(t)\rangle_{u,\mathbf{k}_0}$, and $\langle VW(t)V\rangle_{u,\mathbf{k}_0}$. At later times $t =$ 2 ms and $t = 5$ ms, as shown in Figs. 1(d) and 1(e), the information that V had been applied at $j = 1$ has spread over the system, and hence the measurement of W at $j = 5$ is affected. As an effect, the correlations between $\langle W(t)\rangle_{u,\mathbf{k}_0}$, and $\langle VW(t)V\rangle_{u,\mathbf{k}_0}$ decrease with time, as the OTOCs in ergodic systems.

The formal mapping of correlations between expectation values obtained via forward time evolution from randomized initial states and out-of-time-ordered correlation functions has been derived in Ref. [37]. For the local random

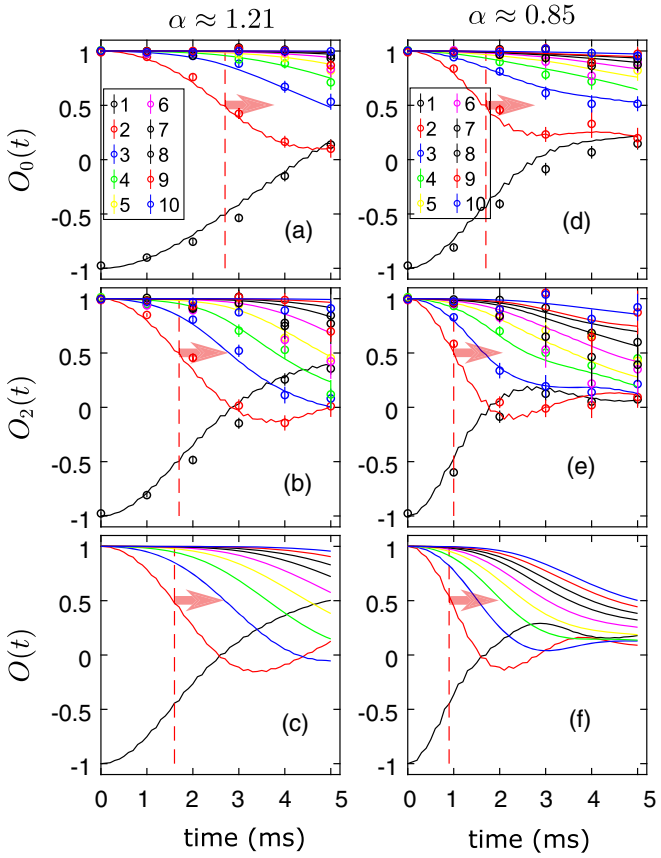

FIG. 2. Out-of-time ordered correlators in a 10-qubit quantum simulator for local operators $V = \sigma_1^z$ and $W(t) = \sigma_j^x(t)$ for $j = 1, 2, \ldots, 10$ (color coded in the figure). On the left panel, estimated OTOCs namely $O_0(t)$ in (a), and $O_2(t)$ in (b) are shown for various interaction times and qubits at interaction exponent $\alpha = 1.21$ and $J_0 = 2\pi \times 30.13$ Hz and $B = 2\pi \times 1.5$ kHz. On the right panel, measurement of OTOCs at $\alpha = 0.85$, $J_0 = 2\pi \times 40.78$ Hz and $B = 2\pi \times 1.5$ kHz. Here circles are experimental points and lines are numerical results for the experimental parameters. (c) and (f) are the exact OTOCs $O(t) = O_{10}(t)$ simulated for the aforementioned parameters. Error bars associated with the experimental measurements are of the size of the symbols and they are deduced by the Jackknife sampling method. Here, red arrows indicate direction of propagation of the *operator wave front* and corresponding vertical dashed lines indicate the times when OTOCs decay to 0.5 (see main text for a detailed discussion).

unitaries employed here, the first part of the protocol [Fig. 1(a)] is to this end repeated (with the same unitaries u) for a set $E_n = \{\mathbf{k}_0, \ldots, \mathbf{k}_{2^n-1}\}$ ($n = 2$ in the context of this work, see below) of initial product states $\mathbf{k} \in E_n$ to obtain estimations of $\langle W(t)\rangle_{u,\mathbf{k}} = \langle \mathbf{k}|u^\dagger W(t) u|\mathbf{k}\rangle$ for all $\mathbf{k} \in E_n$. Here, $\mathbf{k}_s = (k_{s,1}, \ldots, k_{s,N})$ with $k_{s,i} \in \{0, 1\}$ is given by the reverse N-bit binary representation of s, e.g., $\mathbf{k}_0 = (0, 0, \ldots, 0)$, $\mathbf{k}_1 = (1, 0, \ldots, 0)$, $\mathbf{k}_2 = (0, 1, 0, \ldots, 0)$, $\mathbf{k}_3 = (1, 1, 0, \ldots, 0)$ [37]. The summed correlations $\overline{\langle W(t)\rangle_{u,\mathbf{k}} \langle VW(t)V\rangle_{u,\mathbf{k}_0}}$ for all $\mathbf{k} \in E_n$ map then to "modified" OTOCs [37]

$$O_n(t) = \frac{\sum_{\mathbf{k}\in E_n} (-2)^{-D[\mathbf{k}_0,\mathbf{k}]} \overline{\langle W(t)\rangle_{u,\mathbf{k}} \langle VW(t)V\rangle_{u,\mathbf{k}_0}}}{\sum_{\mathbf{k}\in E_n} (-2)^{-D[\mathbf{k}_0,\mathbf{k}]} \overline{\langle W(t)\rangle_{u,\mathbf{k}} \langle W(t)\rangle_{u,\mathbf{k}_0}}}, \quad (3)$$

for $n \in \{0, \ldots, N\}$ and $\overline{\ldots}$ the ensemble average over the random unitaries u. Here, $D[\mathbf{k}_0, \mathbf{k}]$ is the Hamming distance between $\mathbf{k}_0$ and $\mathbf{k}$, i.e., the number of spin flips to transfer $|\mathbf{k}_0\rangle$ into $|\mathbf{k}\rangle$. As shown in Ref. [37] and the Supplemental Material [53], the modified OTOCs $O_n(t)$, with $n = 0, 1, \ldots, N$, represent a series with fast convergence to $O(t)$ with increasing n, in particular $O_N(t) = O(t)$. This means that, to obtain a quantitative measure of the OTOC $O(t)$, the modified OTOCs $O_0(t)$, $O_1(t)$,..., should be measured (with increasing experimental effort) until convergence to $O(t)$. These convergence aspects are discussed in details in Ref. [37] in the context of several physical examples. In our case, we obtain approximate convergence to $O(t)$ at $n = 2$ (see below and [53]). Note that the lowest order modified OTOC, $O_0(t)$, has been measured using this method in a four qubit NMR system [60].

Measurement of OTOCs.—We now present measurements of the modified OTOCs $O_n(t)$ for $n = 0$, 2 for two values of the power law exponent $\alpha = 1.21$ (long-range interaction), and 0.85 (corresponding to a very long-range interaction) and demonstrate the fast convergence to $O(t)$ by a comparison to numerical simulations. For our Hamiltonian evolution with long-range interactions, the operator wave front is not expected to spread in a purely ballistic manner and the shape of the spatial-temporal profile of time ordered [11,12] and out-of-time ordered correlations [38–43] is the matter of current theoretical investigations. In Figs. 2(a) and 2(b), the measured OTOCs $O_0(t)$, $O_2(t)$ (circles) are plotted as a function of time t after the quantum quench at $\alpha = 1.21$, which we compare with numerical simulations (solid lines) assuming unitary time evolution. The error bars are obtained via the Jackknife method [61]. The exact OTOC $O(t)$ calculated from Eq. (3) is shown in Fig. 2(c). All two measured OTOCs display the same qualitative behavior; initially near-perfect (anti-) correlations exist for measurements of $W = \sigma_j^x$ performed at ion $j > 1$ ($j = 1$, respectively) and hence reveal spatiotemporal profiles of the OTOCs in the long-range interacting system. This is described as wave front propagation of local perturbation from the causal site, i.e., the site at which $V(0)$ operator is encoded, to the effect site where the operator $W(t)$ is measured. For the current studies, the propagation of the wave front is indicated with an arrow in Fig. 2. For $\alpha = 0.85$, Fig. 2 right panel, corresponding to even longer range interactions than the aforementioned case, the dynamics of OTOCs look qualitatively different compared to $\alpha = 1.21$. Particularly, here, the dynamics are faster than in the former case. A detailed discussion of the quantitative differences is given below.

At the quantitative level, two observations are apparent: (i) experimentally measured and theoretically simulated

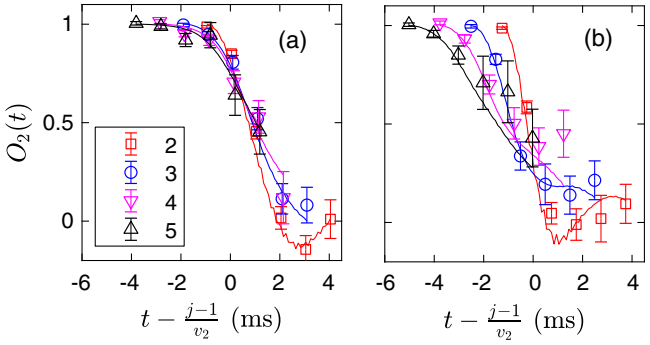

FIG. 3. Out-of-time-ordered correlators versus rescaled time for interactions with power-law exponents (a) $\alpha = 1.21$ and (b) $\alpha = 0.85$ and for $W(t) = \sigma_j^x(t)$ located at spins $j = 2$, 3, 4, 5 (red, blue, pink, black). For (a) $v_2 = (1.0 \pm 0.2) \times 10^3$ s^{-1} and (b) $v_2 = (0.8 \pm 0.2) \times 10^3$ s^{-1} are fitted such that we observe the best possible collapse of the data at a threshold value 0.5 (see the Supplemental Material for details [53]).

OTOCs are, within error limits of the experiment (see the Supplemental Material [53]), in good agreement, implying consistency of the protocol while measuring OTOCs in our system. Furthermore, since the theoretical curves are obtained by simulating unitary dynamics, this demonstrates that the measurement protocol is not affected by decoherence, which appears due to global dephasing in the experiment (see below and the Supplemental Material for further discussion [53]). (ii) $O_0(t)$ describes the same qualitative behavior as $O_2(t)$ but quantitatively differs from the actual OTOC $O(t)$, thus corroborating poor approximations of the OTOCs as predicted by the theory [37]. On the contrary, the OTOC $O_2(t)$ provides a good approximation to $O(t)$, and captures in particular the features of the operator spreading [compare Figs. 2(b) and 2(c), and Figs. 2(e) and 2(f)]. This means that the sampling procedure described above to access the converging series $O_n(t)$ is adapted to our experimental setup [53]. Furthermore, the OTOC measurements slightly deviate at the later times of $t = 4$, 5 ms. This deviation might be due to uncertainties in the determination of the Hamiltonian parameters, which are estimated through measurements of local excitation spread in the ion chain [8]. For further details, see the Supplemental Material [53].

In Figs. 3(a) and 3(b), we study the shape of the spatiotemporal profile of the OTOCs. To this end, we rescale the time axis $t - (j-1)/v_2$, with v_2 chosen such that we observe the best possible collapse of the measured data for various locations j of W at a threshold value of $O_2 = 0.5$ (see the Supplemental Material for details of the fitting procedure [53]). In Fig. 3(a), for a power-law exponent $\alpha = 1.21$, we find that the measured data indeed collapses. Our early time data is thus consistent with a ballistic expansion of the operator wave front, with velocity $v_2 = (1.0 \pm 0.2) \times 10^3$ s^{-1}. We note that, due to finite time and size effects, a slow emergence of superballistic behavior, predicted for large systems and $\alpha = 1.2$ [43], cannot be unambiguously distinguished with our experimental data. In Fig. 3(b), for a power-law exponent $\alpha = 0.85$, we do not observe a collapse of the measured data to a single curve, meaning that the shape of the operator wave front is not conserved over time and space, and therefore that the dynamics is not ballistic. A broadening of the decay of O_2 with time and distance is instead clearly visible. While we emphasize that the spatiotemporal profiles still show some differences when comparing $O_2(t)$ and the exact OTOC $O(t)$, cf. Fig. 2, this strong broadening is consistent with the theoretical prediction for $\alpha < 1$ [43].

Other probes of the scrambling of quantum information.—In generic quantum systems, the scrambling of quantum information does not only manifest itself through the decay of the OTOCs but also through a decrease of statistical moments of the type $\langle W(t)\rangle^2_{u,\mathbf{k}_0}$ [50], and an increase of entanglement entropies [1]. As we show now, the measurement of these two quantities, which are both accessible via randomized measurements, provides us both with evidence of operator spreading that are complementary to OTOCs, and allows us to identify and assess the role of decoherence in our experiment.

The second moment of the expectation value $\overline{\langle W(t)\rangle^2_{u,\mathbf{k}_0}}$ is accessed from statistical autocorrelations of randomized measurements performed on a single system. Its measurement is enabled through the first part of the OTOC protocol [Fig. 1(a)]. Note that $\langle W(t)\rangle^2_{u,\mathbf{k}_0}$ appears also as normalization in the denominator of Eq. (3). As shown in Fig. 4(a), $\langle W(t)\rangle^2_{u,\mathbf{k}_0}$ decreases with time, providing, for unitary dynamics, a direct signature of operator spreading and scrambling [50]. We emphasize that decoherence has a small decreasing effect on the measurement results. This is due to the fact that decoherence drives the system towards a steady state with reduced magnetization. Hence, both, decoherence and scrambling lead to a decay of $\langle W(t)\rangle^2_{u,\mathbf{k}_0}$ with time. In contrast, the OTOC measurement is not affected by decoherence, because our estimation from Eq. (3) is normalized (see Figs. 2–3, for the comparison to unitary theory, and Supplemental Material for simulations with decoherence [53]).

Rényi entanglement entropies quantifying bipartite entanglement are directly related to universal properties of operator spreading [1,26,27], and allow us to observe direct effects of decoherence. The growth of Rényi entanglement entropy was previously measured in Ref. [52] where the effects of decoherence were suppressed by starting the quantum quench from an initial Néel state in a decoherence-free subspace. In contrast, the effects of decoherence can be made visible for an initial condition as in the OTOC measurements, by choosing a random initial state $\bigotimes_{j=1}^{N} u_i|\mathbf{k}_0\rangle$ (with fixed local random unitaries u_i). This state is not protected against decoherence in time evolution. We evolve this state under H, and we measure the second

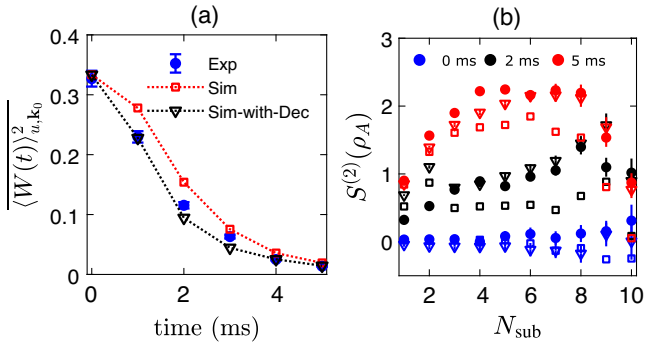

FIG. 4. (a) Time evolution of $\overline{\langle W(t)\rangle^2_{u,\mathbf{k}_0}} = \overline{\langle \sigma^x_j(t)\rangle^2_{u,\mathbf{k}_0}}$, averaged over j (all qubits 1 to 10). Squares (red) and triangles (black) are numerical simulations of unitary dynamics and including decoherence effects, respectively. Dashed lines are guides to the eye. (b) Additionally, Rényi entropy measurements (in circles) are carried out at $t = 0$ (blue), 2 ms (black) and 5 ms (red) for partitions of the form $A = \{1, \ldots, N_{\mathrm{sub}}\}$. Squares and triangles are theoretical simulations without and with decoherence, respectively. The experimental and simulation parameters for studies presented in (a) and (b) are $\alpha = 1.21$, $J_0 = 2\pi \times 30.13$ Hz, and $B = 2\pi \times 1.5$ kHz.

Rényi entropy of the final state, and of reduced density matrices of arbitrary partitions A following Refs. [52,62]. Figure 4(b) shows an increase of the entropy of the total system to around $S^{(2)}(\rho_A) = -\log_2 \mathrm{Tr}[\rho_A^2] = 0.8$ at $t = 2$ ms and $t = 5$ ms, signaling the presence of decoherence, and in quantitative agreement with our numerical simulations [53]. However, the entropy of the subsystems acquires even higher values, which demonstrates the presence of bipartite entanglement [52] associated with operator spreading.

Conclusion and outlook.—We have presented measurements of out-of-time ordered correlators in a system of trapped ions with power-law interactions of tunable range. We have demonstrated how the "wave front" of a local operator propagates in such systems, leading to spatial delocalization of quantum information, and scrambling. The key ingredients of the utilized measurement protocol are randomized measurements which can be implemented with current state-of-the-art technology in various synthetic quantum systems. Their usability is not only feasible with trapped ions but also with Rydberg atoms, optical cavity systems, and superconducting qubits, hence advocating for a powerful and generic method to probe quantum dynamics. The ability to access (modified-)OTOCs in various setups, and their convergence to the exact ones, motivates new approaches to engineer various types of quantum dynamics, in particular in the situation of "fast scrambling" relevant to quantum gravity [63–65] and "out-of-equilibrium" dynamics in lattice systems [6].

We thank J. Bollinger, P. Hrmo, L. K. Joshi, C. Monroe and his group, F. Pollmann, A. Rey, and J. Ye for discussions, and L. Sieberer and N. Yao for their contributions to the theory proposal. The project leading to this application has received funding from the European Research Council (ERC) under the European Union's Horizon 2020 research and innovation programme (Grant Agreement No. 741541), and from the European Union's Horizon 2020 research and innovation programme under Grant Agreements No. 817482 (PASQuanS) and No. 731473 (QuantERA via QTFLAG). Furthermore, this work was supported by the Simons Collaboration on Ultra-Quantum Matter, which is a grant from the Simons Foundation (651440, P. Z.) and LASCEM by AFOSR No. 64896-PH-QC. We acknowledge support by the ERC Synergy Grant UQUAM and by the Austrian Science Fund through the SFB BeyondC (F71). Numerical simulations were realized with QuTiP [66].

[1] R. J. Lewis-Swan, A. Safavi-Naini, A. M. Kaufman, and A. M. Rey, Nat. Rev. Phys. **1**, 627 (2019).
[2] K. A. Landsman, C. Figgatt, T. Schuster, N. M. Linke, B. Yoshida, N. Y. Yao, and C. Monroe, Nature (London) **567**, 61 (2019).
[3] C. Muschik, M. Heyl, E. Martinez, T. Monz, P. Schindler, B. Vogell, M. Dalmonte, P. Hauke, R. Blatt, and P. Zoller, New J. Phys. **19**, 103020 (2017).
[4] C. Kokail, C. Maier, R. van Bijnen, T. Brydges, M. K. Joshi, P. Jurcevic, C. A. Muschik, P. Silvi, R. Blatt, C. F. Roos, and P. Zoller, Nature (London) **569**, 355 (2019).
[5] L. D'Alessio, Y. Kafri, A. Polkovnikov, and M. Rigol, Adv. Phys. **65**, 239 (2016).
[6] J. Eisert, M. Friesdorf, and C. Gogolin, Nat. Phys. **11**, 124 (2015).
[7] M. Cheneau, P. Barmettler, D. Poletti, M. Endres, P. Schauß, T. Fukuhara, C. Gross, I. Bloch, C. Kollath, and S. Kuhr, Nature (London) **481**, 484 (2012).
[8] P. Jurcevic, B. P. Lanyon, P. Hauke, C. Hempel, P. Zoller, R. Blatt, and C. F. Roos, Nature (London) **511**, 202 (2014).
[9] P. Richerme, Z.-X. Gong, A. Lee, C. Senko, J. Smith, M. Foss-Feig, S. Michalakis, A. V. Gorshkov, and C. Monroe, Nature (London) **511**, 198 (2014).
[10] E. H. Lieb and D. W. Robinson, Commun. Math. Phys. **28**, 251 (1972).
[11] P. Hauke and L. Tagliacozzo, Phys. Rev. Lett. **111**, 207202 (2013).
[12] J. Schachenmayer, B. P. Lanyon, C. F. Roos, and A. J. Daley, Phys. Rev. X **3**, 031015 (2013).
[13] S. H. Shenker and D. Stanford, J. High Energy Phys. 03 (2014) 067.
[14] E. Lorenz, in *Proceedings of the 139th Meeting of AAAS Section on Environmental Sciences, New Approaches to Global Weather: GARP* (1972).
[15] S. Sachdev and J. Ye, Phys. Rev. Lett. **70**, 3339 (1993).
[16] A. Kitaev, A simple model of quantum holography, in *Proceedings at KITP, 2015* (2015).
[17] P. Hayden and J. Preskill, J. High Energy Phys. 09 (2007) 120.
[18] J. Maldacena, S. H. Shenker, and D. Stanford, J. High Energy Phys. 08 (2016) 106.

[19] P. Hosur, X.-L. Qi, D. A. Roberts, and B. Yoshida, J. High Energy Phys. 02 (2016) 004.

[20] D. A. Roberts and B. Yoshida, J. High Energy Phys. 04 (2017) 121.

[21] S. Banerjee and E. Altman, Phys. Rev. B **95**, 134302 (2017).

[22] D. A. Roberts and B. Swingle, Phys. Rev. Lett. **117**, 091602 (2016).

[23] M. Blake, Phys. Rev. Lett. **117**, 091601 (2016).

[24] Note that, in general, $O(t) = \mathrm{Tr}[\rho W(t) V W(t) V]$ for some state ρ. Here, we consider the infinite temperature OTOC $\rho = \mathbb{1}/D$.

[25] A. Bohrdt, C. B. Mendl, M. Endres, and M. Knap, New J. Phys. **19**, 063001 (2017).

[26] A. Nahum, S. Vijay, and J. Haah, Phys. Rev. X **8**, 021014 (2018).

[27] C. W. von Keyserlingk, T. Rakovszky, F. Pollmann, and S. L. Sondhi, Phys. Rev. X **8**, 021013 (2018).

[28] R. Fan, P. Zhang, H. Shen, and H. Zhai, Sci. Bull. **62**, 707 (2017).

[29] Y. Huang, Y.-L. Zhang, and X. Chen, Ann. Phys. (Berlin) **529**, 1600318 (2017).

[30] X. Chen, T. Zhou, D. A. Huse, and E. Fradkin, Ann. Phys. (Berlin) **529**, 1600332 (2017).

[31] M. Heyl, F. Pollmann, and B. Dóra, Phys. Rev. Lett. **121**, 016801 (2018).

[32] S. Xu and B. Swingle, Phys. Rev. X **9**, 031048 (2019).

[33] J. Couch, S. Eccles, P. Nguyen, B. Swingle, and S. Xu, arXiv:1908.06993.

[34] M. Gärttner, J. G. Bohnet, A. Safavi-Naini, M. L. Wall, J. J. Bollinger, and A. M. Rey, Nat. Phys. **13**, 781 (2017).

[35] K. X. Wei, C. Ramanathan, and P. Cappellaro, Phys. Rev. Lett. **120**, 070501 (2018).

[36] J. Li, R. Fan, H. Wang, B. Ye, B. Zeng, H. Zhai, X. Peng, and J. Du, Phys. Rev. X **7**, 031011 (2017).

[37] B. Vermersch, A. Elben, L. M. Sieberer, N. Y. Yao, and P. Zoller, Phys. Rev. X **9**, 021061 (2019).

[38] M. Foss-Feig, Z.-X. Gong, C. W. Clark, and A. V. Gorshkov, Phys. Rev. Lett. **114**, 157201 (2015).

[39] T. Matsuta, T. Koma, and S. Nakamura, Ann. Henri Poincaré **18**, 519 (2017).

[40] M. C. Tran, A. Y. Guo, Y. Su, J. R. Garrison, Z. Eldredge, M. Foss-Feig, A. M. Childs, and A. V. Gorshkov, Phys. Rev. X **9**, 031006 (2019).

[41] D. V. Else, F. Machado, C. Nayak, and N. Y. Yao, Phys. Rev. A **101**, 022333 (2020).

[42] D. J. Luitz and Y. Bar Lev, Phys. Rev. A **99**, 010105(R) (2019).

[43] T. Zhou, S. Xu, X. Chen, A. Guo, and B. Swingle, Phys. Rev. Lett. **124**, 180601 (2020).

[44] B. Swingle, G. Bentsen, M. Schleier-Smith, and P. Hayden, Phys. Rev. A **94**, 040302(R) (2016).

[45] N. Y. Yao, F. Grusdt, B. Swingle, M. D. Lukin, D. M. Stamper-Kurn, J. E. Moore, and E. A. Demler, arXiv:1607.01801.

[46] G. Zhu, M. Hafezi, and T. Grover, Phys. Rev. A **94**, 062329 (2016).

[47] B. Swingle and N. Yunger Halpern, Phys. Rev. A **97**, 062113 (2018).

[48] B. Yoshida and N. Y. Yao, Phys. Rev. X **9**, 011006 (2019).

[49] J. R. González Alonso, N. Yunger Halpern, and J. Dressel, Phys. Rev. Lett. **122**, 040404 (2019).

[50] X.-L. Qi, E. J. Davis, A. Periwal, and M. Schleier-Smith, arXiv:1906.00524.

[51] A. Elben, B. Vermersch, M. Dalmonte, J. I. Cirac, and P. Zoller, Phys. Rev. Lett. **120**, 050406 (2018).

[52] T. Brydges, A. Elben, P. Jurcevic, B. Vermersch, C. Maier, B. P. Lanyon, P. Zoller, R. Blatt, and C. F. Roos, Science **364**, 260 (2019).

[53] See the Supplemental Material at http://link.aps.org/supplemental/10.1103/PhysRevLett.124.240505 for information regarding experimental details, error analysis, and numerical simulations, which includes Refs. [54–57].

[54] R. Blume-Kohout, J. K. Gamble, E. Nielsen, J. Mizrahi, J. D. Sterk, and P. Maunz, arXiv:1310.4492v1.

[55] E. Nielsen, K. Rudinger, J. K. Gamble, and R. Blume-Kohout, pygsti v. 0.9.7.5: A python implementation of gate set tomography, 2019.

[56] R. Blume-Kohout, J. King Gamble, E. Nielsen, K. Rudinger, J. Mizrahi, K. Fortier, and P. Maunz, Nat. Commun. **8**, 1 (2017).

[57] P. A. Barton, C. J. S. Donald, D. M. Lucas, D. A. Stevens, A. M. Steane, and D. N. Stacey, Phys. Rev. A **62**, 032503 (2000).

[58] F. Mezzadri, Not. Am. Math. Soc. **54**, 592 (2007); arXiv:math-ph/0609050.

[59] A. Elben, B. Vermersch, R. van Bijnen, C. Kokail, T. Brydges, C. Maier, M. K. Joshi, R. Blatt, C. F. Roos, and P. Zoller, Phys. Rev. Lett. **124**, 010504 (2020).

[60] X. Nie, Z. Zhang, X. Zhao, T. Xin, D. Lu, and J. Li, arXiv:1903.12237.

[61] J. Shao and D. Tu, *The Jackknife and Bootstrap* (Springer Science & Business Media, New York, 2012).

[62] A. Elben, B. Vermersch, C. F. Roos, and P. Zoller, Phys. Rev. A **99**, 052323 (2019).

[63] I. Danshita, M. Hanada, and M. Tezuka, Prog. Theor. Exp. Phys. (**2017**) 083I01.

[64] J. Marino and A. M. Rey, Phys. Rev. A **99**, 051803(R) (2019).

[65] G. Bentsen, T. Hashizume, A. S. Buyskikh, E. J. Davis, A. J. Daley, S. S. Gubser, and M. Schleier-Smith, Phys. Rev. Lett. **123**, 130601 (2019).

[66] J. R. Johansson, P. Nation, and F. Nori, Comput. Phys. Commun. **183**, 1760 (2012).